

Two polypyridyl copper(II) complexes: synthesis, crystal structure and interaction with DNA and serum protein *in vitro*†

Cite this: *New J. Chem.*, 2014, **38**, 955

Xiao-Fei Zhao,^{‡,ab} Yan Ouyang,^{‡,a} Yan-Zhao Liu,^a Qiao-Juan Su,^a He Tian,^a Cheng-Zhi Xie^a and Jing-Yuan Xu^{*a}

Two polypyridyl copper(II) complexes, [Cu(acac)(*p*-CPIP)(CH₃OH)](NO₃) (**1**) and [Cu(acac)(*o*-NPIP)(NO₃)] (**2**) (acac = acetylacetonate, *p*-CPIP = 2-(4-chlorophenyl)imidazo[4,5-*f*]1,10-phenanthroline, *o*-NPIP = 2-(2-nitrophenyl)imidazo[4,5-*f*]1,10-phenanthroline), have been synthesized and characterized by single-crystal analysis, IR and electronic spectroscopy. X-ray analyses reveal that both **1** and **2** possess a triclinic crystal system with *Pmn*1 and mononuclear five-coordinated square pyramidal geometry, which were further linked to a one-dimensional structure through π - π stacking and intermolecular hydrogen bonds. The interaction of the Cu(II) complex with calf thymus DNA (CT-DNA) was investigated by UV-visible and fluorescence emission spectrometry, as well as agarose gel electrophoresis. The apparent binding constant (K_{app}) values of $2.47 \times 10^4 \text{ M}^{-1}$ for **1** and $3.04 \times 10^4 \text{ M}^{-1}$ for **2** suggest moderate intercalative binding mode between the complexes and DNA. Both complexes displayed efficient oxidative cleavage of supercoiled DNA in the presence of external agents. In addition, fluorescence spectrometry of bovine serum albumin (BSA) with the complexes showed that the quenching mechanism of **1** might be a dynamic procedure, while **2** showed a combined dynamic and static quenching mechanism. For both **1** and **2**, the number of binding sites was about one for BSA. Moreover, synchronous fluorescence spectral experiments revealed that **1** and **2** affect the microenvironment of tryptophan residues of BSA.

Received (in Victoria, Australia)
16th September 2013,
Accepted 2nd December 2013

DOI: 10.1039/c3nj01107k

www.rsc.org/njc

Introduction

In recent years, metal complexes that are capable of cleaving DNA under physiological conditions have attracted increasing attention not only because of their potential applications in artificial nucleic acid chemistry, but also because of the development of metal-based anticancer agents.^{1–6} As we know well, cisplatin as an efficient clinical chemotherapeutic agent represents a major landmark in the history of metal-based anticancer drugs. However, cisplatin is associated with acquired resistance and the limited spectrum of the anticancer activity, which has stimulated us to develop more effective, less toxic, target specific, and preferably noncovalently binding anticancer drugs.^{7,8} Heretofore, many studies have suggested that DNA is the primary intracellular target of

anticancer drugs, because the interaction between the small molecule and DNA can cause DNA damage in cancer cells.^{9,10} Metal complexes containing a planar heterocyclic aromatic ligand, such as polypyridyl, have been at the forefront of these investigations owing to their unusual electronic properties, diverse chemical reactivity and peculiar structures, which resulted in their binding to DNA by many modes such as electrostatic, groove and intercalative binding.¹¹ In general, polypyridyl metal complexes displayed the intercalative binding modes to DNA for their large planar ligands and π - π overlapping interaction.^{12,13} Over the past few decades, it has been considered that the polypyridyl metal complexes can probe nonradioactive nucleic acid and effectively cleave DNA.¹⁴ In general, the DNA cleavage mode mainly contained oxidative cleavage, photocleavage and hydrolytic cleavage.¹⁵ While most studies suggested that polypyridyl transition metal complexes exhibit photocleavage ability towards DNA.¹⁶ However, studies on those polypyridyl complexes hitherto have mainly focused on fully planar ligands, and as far as we know, the complexes containing such ligand derivatives with diverse substituents are seldom investigated.¹⁷ In fact, introducing substituents could improve the cleavage ability of polypyridyl complexes to bind to DNA, such as *o*-NPIP based on the almost coplanar ligand of (2-phenyl)imidazo[4,5-*f*]1,10-phenanthroline (PIP).^{18,19}

^a Tianjin Key Laboratory on Technologies Enabling Development of Clinical Therapeutics and Diagnostics, School of Pharmacy, Tianjin Medical University, Tianjin 300070, P. R. China. E-mail: xujingyuan@tmu.edu.cn

^b Department of Pharmacy, The Second Affiliated Hospital of Xing Tai Medical College in Hebei, Xingtai, 054000, P. R. China

† Electronic supplementary information (ESI) available. CCDC 920155 for the *p*-CPIP ligand, 801495 for **1** and 859802 for **2**. For ESI and crystallographic data in CIF or other electronic format see DOI: 10.1039/c3nj01107k

‡ These authors contributed equally to this work.

The ruthenium(II) complex with *o*-NPIP has been synthesized and exhibited good DNA binding ability and photocleavage ability.²⁰ Inspired by these results, we synthesized a ligand 2-(4-chlorophenyl)imidazo[4,5-*f*]-1,10-phenanthroline (*p*-CPIP) and two complexes [Cu(acac)(*p*-CPIP)(CH₃OH)](NO₃) and [Cu(acac)(*o*-NPIP)(NO₃)]. The choice of Cu was based on the fact that copper, as a fundamental micronutrient for human, has bioessential activity and oxidative nature, which has attracted numerous inorganic chemists to find the potential medical applications of copper complexes.²¹ Since Sigman found the “chemical nuclease” activity of [Cu(phen)]²⁺ (phen = 1,10-phenanthroline),¹⁴ Cu(II) complexes have been widely used as DNA footprinting agents, as structural probes for DNA and as potential anticancer drugs. Especially, Cu(II) complexes containing planar ligands have received considerable current interest because of their strong DNA binding ability and DNA cleavage activities *via* oxidation and photocleavage.²² On the other hand, it is well known that serum albumins, as the most abundant proteins in the circulatory system, act as transporters and disposers of many endogenous and exogenous compounds,²³ including drugs and nutrients, mostly through the formation of noncovalent complexes as specific binding sites. Therefore, the absorption, distribution, metabolism and excretion properties, as well as the stability and toxicity of chemical substances, can be significantly affected by their binding activities to serum albumins.²⁴ As a kind of serum albumin, bovine serum albumin (BSA) has been extensively studied owing to its structural homology with human serum albumin (HSA).²⁵ Furthermore, administration of platinum-based antitumor agents injected intravenously prompts us to investigate the binding of this kind of complexes to BSA. As reported, 65–98% of platinum is bound by proteins in blood plasma in one day after cisplatin treatment.²⁶ Such interaction between platinum and proteins would lead to inactivation of drugs, thus affecting the therapeutic dose of drugs transferred to their target positions.^{27,28} Therefore such a study is of special interest in the evaluation of metal drugs.

Here, we report the synthesis, structural characterization and biological properties of two polypyridyl Cu(II) complexes, [Cu(acac)(*p*-CPIP)(MeOH)](NO₃) (**1**) and [Cu(acac)(*o*-NPIP)(NO₃)] (**2**). The results show that the two complexes can efficiently bind to DNA and BSA and cleave DNA in the presence of external agents.

Experimental

Materials and physical measurements

All chemicals were purchased from commercial sources and used without further purification. Calf thymus DNA (CT-DNA), ethidium bromide (EB), pUC19 DNA and BSA were from Sigma. Tris-HCl buffer solution was prepared using triple-distilled water.

CT-DNA stock solution was prepared by dissolving into deionized sonicated triple-distilled water, and kept at 4 °C for no longer than a week. The UV absorbance at 260 and 280 nm of CT-DNA solution in Tris-buffer gives a ratio of 1.8–1.9, indicating that the DNA was free of proteins.²⁹

Elemental analysis of C, H and N was carried out on a Perkin-Elmer analyzer model 240. ¹H NMR spectra were recorded on a

Bruker AVANCE III 400 spectrometer with TMS as internal standard and (CD₃)₂SO as solvent. Infrared spectroscopy on KBr pellets was performed on a Bruker Vector 22 FT-IR spectrophotometer in the 4000–400 cm⁻¹ regions. The fluorescence spectral data were obtained on a MPF-4 fluorescence spectrophotometer at room temperature. The Gel Imaging and documentation DigiDoc-It System were assessed by Labworks Imaging and Analysis Software (UVI, UK). The electronic spectra were recorded on a HITACHI spectrophotometer. Emission spectra were recorded on a Shimadzu RF-5301 fluorescence spectrophotometer with excitation at 510 nm.

Syntheses of ligands

2-(4-Chlorophenyl)imidazo[4,5-*f*]-1,10-phenanthroline (*p*-CPIP). The polypyridyl ligand of *p*-CPIP was obtained according to the procedure in ref. 30. A mixture of 4-chlorobenzaldehyde (0.28 g, 2 mmol), 1,10-phenanthroline-5,6-dione (0.21 g, 1 mmol) and glacial acetic acid (15 mL) was refluxed for about 3 h, then cooled to room temperature and diluted with water (40 mL). Dropwise addition of concentrated aqueous ammonia gave yellow precipitates, which were collected and washed with water. The crude products were purified by silica gel filtration (60–100 mesh, ethanol). The principal yellow band was collected and solvent was removed by rotary evaporation. The products were obtained, and then dried at 50 °C *in vacuo*. Then, the products were dissolved in ethanol and kept at room temperature for slow evaporation, and gave the yellow crystals of 2-(4-chlorophenyl)imidazo[4,5-*f*]-1,10-phenanthroline after two days. Yield 0.489 g, 74.1%. Anal. calc. for C₂₁H₁₇ClN₄O: C, 67.79, H, 4.40, N, 14.49%, found: C, 67.77; H, 4.39; N, 14.51%. FT-IR (KBr, cm⁻¹): 2964(m), 1475(vs), 1446(vs), 1377(m), 1100(m), 1067(w), 1048(m), 1012(w), 841(m), 801(m), 737(m), 686(m) cm⁻¹. ¹H NMR[(CD₃)₂SO]: δ 13.81 (s, 1H), 9.04 (d, 2H), 8.91–8.87 (m, 2H), 8.30–8.28 (d, 2H), 7.87–7.81 (m, 2H), 7.71–7.69 (d, 2H).

2-(2-Nitrophenyl)imidazo[4,5-*f*]-1,10-phenanthroline (*o*-NPIP). This compound was synthesized in a similar way to the above one except for using 2-nitrobenzaldehyde (0.302 g, 2 mmol) instead of 4-chlorobenzaldehyde. Yield 0.469 g, 68.1%. Anal. calc. for C₁₉H₁₁N₅O₂: C, 66.09, H, 3.19, N, 20.29%, found: C, 66.08, H, 3.17, N, 20.30%. FT-IR (KBr, cm⁻¹): 3006(m), 1537(vs), 1364(m), 808(w), 739(m), 721(w), 648(w) cm⁻¹. ¹H NMR[(CD₃)₂SO]: δ 13.83 (s, 1H), 9.05 (d, 1H), 9.01 (d, 1H), 8.95 (d, 1H), 8.86 (d, 1H), 7.94 (d, 1H), 7.89–7.80 (m, 2H), 7.70 (d, 1H) and 7.60–7.53 (m, 2H).

Syntheses of complexes

[Cu(acac)(*p*-CPIP)(MeOH)](NO₃) (1**).** The *p*-CPIP (0.066 g, 0.2 mmol) and Cu(NO₃)₂·3H₂O (0.0429 g, 0.2 mmol) were dissolved in MeOH and EtOH (v:v = 1:1) (20 mL). The solution was refluxed for half an hour, and then acetylacetonate (0.09 mL) was added. The complex was refluxed for 3 h giving a clean blue solution. The reaction mixture was filtered off and kept at room temperature for slow evaporation, and the blue crystals of [Cu(acac)(*p*-CPIP)(MeOH)](NO₃) suitable for X-ray analysis were collected after one day. Yield: 0.0649 g, 57% for **1**. Elemental analysis (%): calc. for C₂₅H₂₂ClCuN₅O₆: C, 51.06, H, 3.74, N, 11.92%, found: C, 51.08, H, 3.73, N, 11.91%. FT-IR (KBr, cm⁻¹):

3078m(br), 2974m(br), 1582(v)s, 1520(vs), 1455(vs), 1378vs(br), 1278s(br), 1101(m), 1075(m), 1014(s), 945(w), 843(m), 813(m), 771(w), 730(m) cm^{-1} .

[Cu(acac)(*o*-NPIP)(NO₃)] (2). The blue complex **2** was synthesized in a manner analogous to complex **1** mentioned above, with *o*-NPIP (0.0624 g, 0.2 mmol) in place of *p*-CPIP (0.066 g, 0.2 mmol), and 20 mL of MeOH was employed as solvent. Yield: 0.061 g, 52% for **2**. Elemental analysis (%): calc. for C₄₈H₃₆Cu₂N₁₂O₁₄: C, 50.88, H, 3.18, N, 14.84%; found C, 50.86, H, 3.17, N, 14.86%. FT-IR (KBr, ν/cm^{-1}): 2821(w), 1613(w), 1540(m), 1531(m), 1514(s), 1442(m), 1378(m), 1304(m), 1023(w), 816(w), 774(w), 728(w), 697(w) cm^{-1} .

X-ray structure determination

Suitable single crystals of ligand *p*-CPIP, complexes **1** and **2** were used for X-ray diffraction analyses by mounting on the tip of a glass fiber in air. Crystal data were collected at 298(2) K for *p*-CPIP, 293(2) K for **1** and 113(2) K for **2**, using a Bruker SMART CCD 1000 diffractometer. Diffraction intensities for the three compounds were collected by using the ω -scan technique. The structures were solved by direct methods using the program SHELXS-97³¹ and subsequent Fourier difference techniques, and refined anisotropically by full-matrix least-squares on F^2 using SHELXL-97. All the nonhydrogen atoms were refined anisotropically and all the hydrogen atoms were located in the Fourier difference maps.

Measurements

DNA-binding studies. Using the UV-vis spectral method, the relative binding of two complexes to CT-DNA was measured in 5 mM Tris-HCl/50 mM NaCl buffer (pH = 7.2). The concentration of CT-DNA was determined from its absorption intensity at 260 nm with a molar extinction coefficient of 6600 $\text{M}^{-1} \text{cm}^{-1}$.³² The absorption spectra of two complexes binding to CT-DNA were recorded by adding CT-DNA solution at different concentrations (0–35 μM) to the samples of **1** (45.5 μM) and **2** (47.6 μM) in 10% DMF. Fluorescence quenching experiments were carried out by adding **1** or **2** at different concentrations to the EB-bound CT-DNA solution (EB = 5×10^{-5} M and CT-DNA = 100×10^{-5} M) in 5 mM Tris-HCl/50 mM NaCl buffer (pH = 7.2). All the fluorescence intensities were obtained at room temperature with excitation at 510 nm and emission at 592 nm.

DNA cleavage and mechanistic studies. The DNA cleavage experiments were done by agarose gel electrophoresis, which was performed by the following literature method. pUC19 DNA in 50 mM Tris-HCl/18 mM NaCl buffer (pH = 7.2) was treated with complexes **1** and **2** in the absence of additives, respectively. The samples were incubated at 37 °C for 3 h, and 4 μL of loading buffer was added after incubation. Then the samples were electrophoresed for 0.5 h at 100 V on 0.1% ethidium bromide (EB) gel in TAE buffer. After electrophoresis, bands were visualized under UV light and photographed. Cleavage mechanistic investigation of pUC19 DNA was done by adding different scavengers, such as DMSO, NaN₃, superoxide dismutase enzyme (SOD), EDTA, KI and L-histidine, to the different concentrations of complexes, and then the samples were incubated by the same method described for DNA cleavage, and further analysis was carried out by the above method.

BSA binding studies. The protein (BSA) binding experiments were performed using fluorescence quenching and UV spectrophotometry. The protein was prepared in the buffer solution (containing 0.01 M Na₂HPO₄ and NaH₂PO₄ in pure aqueous medium at pH = 7.2). BSA solution concentration was controlled at 5×10^{-7} M (based on the molecular weight of BSA 66 000), and the solutions were kept in the dark at 277 K for 24 h. Fluorescence quenching measurements were done by keeping the concentration of BSA constant while adding the increasing concentration of **1** and **2** at different temperatures (288, 298 and 310 K), respectively. Fluorescence spectra were recorded at an excitation wavelength of 290 nm and the emission spectra from 300 to 500 nm. Synchronous fluorescence spectral experiments were carried out by the same method as above while keeping the D values ($\Delta\lambda$) between excitation and emission wavelengths, which are stabilized at 15 and 60 nm, respectively, at room temperature. UV spectrometry was performed using a HITACHI spectrophotometer equipped with a 1 cm quartz cell. Absorption titration experiments were done by keeping the concentration of BSA constant (3×10^{-5} M) while adding the same concentration **1** and **2** solution, respectively. All the data were obtained after each successive addition of BSA solution and equilibration (*ca.* 10 min).

Results and discussion

We synthesized a new *p*-CPIP ligand, and two new complexes **1** and **2** in good yield. The blue crystals of complexes suitable for X-ray analysis were collected after one day. The polypyridyl metal complexes displayed the intercalative binding modes to DNA owing to their large planar ligands to form π - π overlapping interaction.

Crystal structure characterization

The *p*-CPIP ligand and two complexes have been structurally characterized by single crystal X-ray structural analysis (Fig. 1). The details of crystallographic data and structure refinement parameters are provided in Table 1, and the selected bond lengths and angles are listed in Table 2.

The ligand *p*-CPIP crystallizes in the monoclinic crystal system with the $P2_1/c$ space group. The basic unit contains a *p*-CPIP and an ethanol molecule. The *p*-CPIP molecule contains two planes. One is composed of N(1), N(2), N(3) and N(4), and the other is composed of a benzene cycle with the substituent of Cl(1). The basal atoms deviate from their main plane by 0.0161, 0.0133, -0.0161, and -0.0133 Å for N(1), N(2), N(3) and N(4), respectively. And the Cl(1) atom deviates from the benzene ring by -0.0331 Å. The dihedral angle between the two planes is 10.2°.

A perspective view of complex **1** is depicted in Fig. 1. Complex **1** crystallizes in the triclinic crystal system with the $Pmn1$ space group. The copper atom displays a slightly distorted square pyramidal (4 + 1) geometry with $\tau = 0.025$ ($\tau = 0$ for a perfect square pyramidal and 1 for a perfect trigonal-bipyramidal coordination sphere according to the Addison/Reedijk geometric criterion).³³ The basal coordination positions are occupied by N(1) and N(2) from the *p*-CPIP ligand (Cu(1)-N(1) 1.980(6),

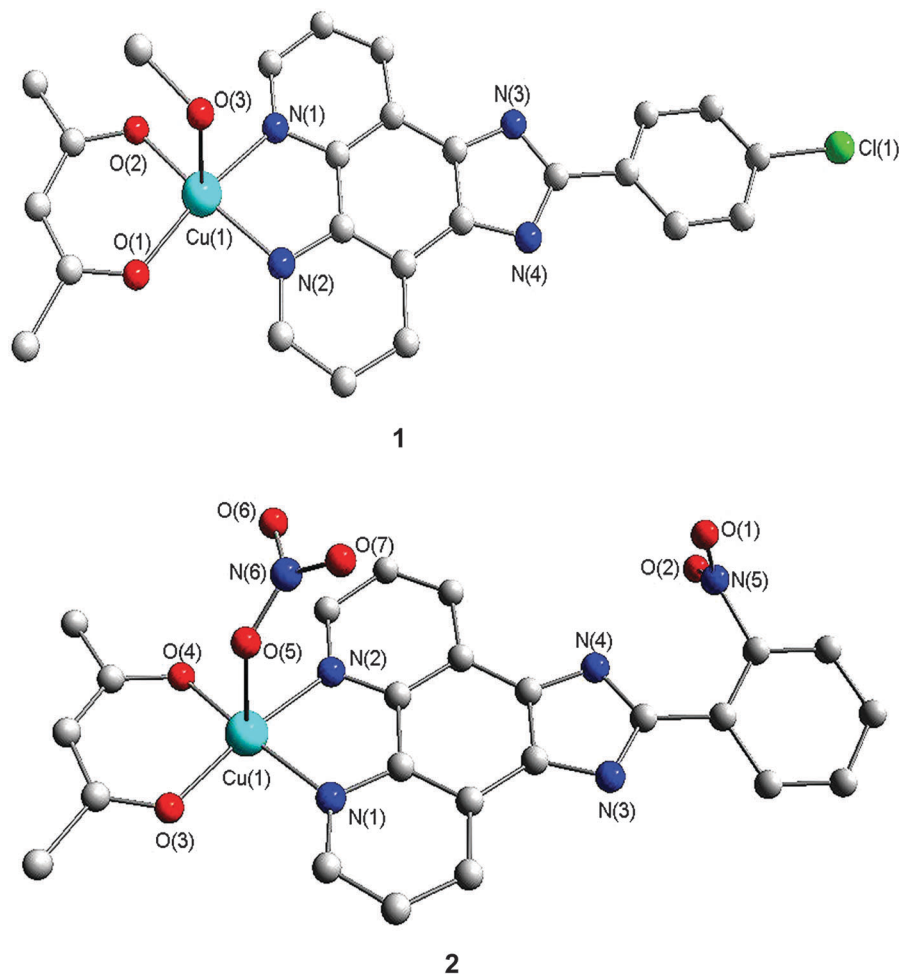


Fig. 1 Crystal structure of $[\text{Cu}(\text{acac})(p\text{-CPIP})(\text{MeOH})](\text{NO}_3)$ (**1**) and $[\text{Cu}(\text{acac})(o\text{-NPIP})](\text{NO}_3)$ (**2**). Hydrogen atoms and solvent molecules are omitted for clarity.

$\text{Cu}(1)\text{-N}(2)$ 1.986(6) Å), and O(1) and O(2) from the acac ligand ($\text{Cu}(1)\text{-O}(1)$ 1.884(5) and $\text{Cu}(1)\text{-O}(2)$ 1.901(5) Å). The basal donor atoms deviate from their main plane by -0.0247 , 0.0245 , -0.0263 and 0.0265 Å for O(1), O(2), N(1) and N(2), respectively, and Cu(1) is displaced out of the plane towards the apex by -0.1160 Å. The apical position is occupied by the O(3) atom of MeOH ($\text{Cu}(1)\text{-O}(3)$, 2.323 Å) with the distance to the plane 2.433 Å. Moreover, there exists one noncoordinated NO_3^- anion in **1**, which can link the H-bonding acceptor by weak interactions to stabilize the structure of the complex. As can be seen from the packing diagram of complex **1** (Fig. S1, ESI[†]), the plane-plane distance of two units is 3.716 Å, showing distinct $\pi\text{-}\pi$ interactions.

Complex **2** crystallizes with two independent molecules in the asymmetric unit, which are almost the same except for slight difference in bond lengths between each other. One $[\text{Cu}(\text{acac})(o\text{-NPIP})](\text{NO}_3)$ unit is depicted in Fig. 1. The coordination environment of the Cu atom is very similar to that of **1**, in which Cu(1) is located in a (4 + 1) environment, showing a slightly distorted square-pyramidal geometry with $\tau = 0.035$. The equatorial plane of Cu(1) is formed by two N atoms of the *o*-NPIP ligand and two O atoms of the acac ligand [$\text{Cu}(1)\text{-O}(4)$ 1.904(3), $\text{Cu}(1)\text{-O}(3)$ 1.914(3), $\text{Cu}(1)\text{-N}(2)$ 2.005(3) and $\text{Cu}(1)\text{-N}(1)$ 2.005(3) Å].

While the basal donor atoms of O(3), O(4), N(1) and N(2) deviate from their mean plane by -0.0298 , 0.0298 , 0.0319 , and -0.0319 Å, respectively. On the whole, complex **2** possesses a planar structure with two N atoms and two O atoms situated at both sides of the Cu(II) ion symmetrically at the same Cu-O bond length of 2.005(3) Å. The NO_3^- anion in **1** is disordered and noncoordinated, but coordinated to the Cu atom in **2**. The packing diagram of **2** (Fig. S1, ESI[†]) shows two kinds of weak interactions between two units: hydrogen bonds and $\pi\text{-}\pi$ interactions. Hydrogen bonds exist between the O atoms of NO_3^- from one unit and N atoms of the *o*-NPIP ligand from the neighboring unit (O(7)-N(3), 2.823 Å). The distances between two mononuclear units are 3.696 and 3.760 Å, respectively, showing distinct $\pi\text{-}\pi$ interactions.

DNA-binding studies

Electronic absorption method. The electronic absorption spectrometry is an effective way to investigate the interactions of complexes with CT-DNA. The absorption spectra of **1** and **2** in the absence and presence of CT-DNA at different concentrations are given in Fig. 2. The results show that **1** has a very strong absorption at *ca.* 283 nm, and **2** exhibits two absorptions

Table 1 Crystal data and structure refinement parameters of the *p*-CPIP ligand, complexes **1** and **2**

| | <i>p</i> -CPIP | 1 | 2 |
|--|--|---|---|
| Formula | C ₂₁ H ₁₇ ClN ₄ O | C ₂₅ H ₂₂ ClCuN ₅ O ₆ | C ₂₄ H ₁₈ CuN ₆ O ₇ |
| Formula weight | 376.84 | 587.48 | 565.99 |
| <i>T</i> /K | 298(2) | 293(2) | 113(2) |
| Crystal system | Monoclinic | Triclinic | Triclinic |
| Space group | <i>P</i> 2 ₁ / <i>n</i> | <i>P</i> $\bar{1}$ | <i>P</i> $\bar{1}$ |
| <i>a</i> /Å | 9.921(2) | 8.586(17) | 8.418(3) |
| <i>b</i> /Å | 11.098(2) | 11.180(2) | 9.753(3) |
| <i>c</i> /Å | 17.289(4) | 13.844(3) | 28.363(10) |
| α /° | 90 | 97.13(3) | 92.028(7) |
| β /° | 97.50 | 104.40(3) | 90.542(6) |
| γ /° | 90 | 94.66(3) | 93.765(8) |
| <i>V</i> /Å ³ | 1887.3(7) | 1268.5(4) | 2322.0(14) |
| <i>Z</i> | 4 | 2 | 4 |
| <i>D</i> _{calc} [g cm ⁻³] | 1.326 | 1.538 | 1.619 |
| μ (Mo-K α) mm ⁻¹ | 0.221 | 1.017 | 1.001 |
| <i>F</i> (000) | 784 | 602 | 1156 |
| θ range for data collection | 3.00 to 27.48 | 3.07 to 25.05 | 2.46 to 28.12 |
| Reflections measured | 18 344 | 7555 | 19 659 |
| Unique reflections | 4323 | 4419 | 8116 |
| <i>R</i> (int) | 0.0646 | 0.0971 | 0.0582 |
| Parameters | 244 | 355 | 685 |
| GOF | 1.166 | 0.972 | 1.027 |
| <i>R</i> ₁ , <i>wR</i> ₂ [<i>I</i> > 2 σ (<i>I</i>)] | 0.0837, 0.1561 | 0.0950, 0.2131 | 0.0544, 0.1122 |
| <i>R</i> ₁ , <i>wR</i> ₂ (all data) | 0.1255, 0.1722 | 0.1818, 0.2538 | 0.0778, 0.1225 |

Table 2 Selected bond lengths [Å] and bond angles [°] of complexes **1** and **2**

| 1 | | | |
|-----------------|------------|-----------------|------------|
| Cu(1)–N(1) | 1.974(7) | Cu(1)–N(2) | 1.990(6) |
| Cu(1)–O(1) | 1.876(6) | Cu(1)–O(2) | 1.896(6) |
| Cu(1)–O(3) | 2.321(6) | | |
| O(1)–Cu(1)–O(2) | 94.6(2) | O(1)–Cu(1)–N(1) | 171.3(3) |
| O(2)–Cu(1)–N(1) | 91.7(3) | O(1)–Cu(1)–N(2) | 91.4(3) |
| O(2)–Cu(1)–N(2) | 169.5(3) | N(1)–Cu(1)–N(2) | 81.4(3) |
| O(1)–Cu(1)–O(3) | 96.9(2) | O(2)–Cu(1)–O(3) | 92.6(2) |
| N(1)–Cu(1)–O(3) | 88.7(3) | N(2)–Cu(1)–O(3) | 95.3(3) |
| 2 | | | |
| Cu(1)–O(4) | 1.904(3) | Cu(1)–O(3) | 1.914(3) |
| Cu(1)–N(1) | 2.004(3) | Cu(1)–N(2) | 2.005(3) |
| Cu(1)–O(5) | 2.320(3) | | |
| O(4)–Cu(1)–O(3) | 94.92(12) | O(4)–Cu(1)–N(2) | 91.49(13) |
| O(3)–Cu(1)–N(2) | 172.61(12) | O(4)–Cu(1)–N(1) | 170.49(12) |
| O(3)–Cu(1)–N(1) | 91.41(12) | N(2)–Cu(1)–N(1) | 81.78(13) |
| O(4)–Cu(1)–O(5) | 97.31(11) | O(3)–Cu(1)–O(5) | 96.37(10) |
| N(2)–Cu(1)–O(5) | 86.44(11) | N(1)–Cu(1)–O(5) | 89.01(12) |

at ca. 257 nm and 290 nm, respectively. All these bands can be attributed to the intraligand π – π^* transition. As the CT-DNA concentration was increased, the absorption spectra of both complexes showed clearly hypochromism and red shift at the maximum peak. A 50.36% hypochromism and a 3 nm red shift at 283 nm for **1**, while a 77.7% hypochromism and a 6 nm red shift at 290 nm for **2** were observed, indicating that both **1** and **2** bound to CT-DNA in intercalative mode. Here we suggest that this hypochromism and red shift should be contributed to the intercalative mode relating to a strong stacking interaction between the planar aromatic chromophore and the base pairs of DNA. Furthermore, the extent of the hypochromism is commonly consistent with the strength of intercalative action.³⁴ In order to elucidate the binding strength of the complexes with DNA,

the binding constant K_b was determined using the following eqn (1):³⁵

$$[\text{DNA}]/(\varepsilon_a - \varepsilon_f) = [\text{DNA}]/(\varepsilon_b - \varepsilon_f) + 1/K_b(\varepsilon_b - \varepsilon_f) \quad (1)$$

where [DNA] is the concentration of DNA, ε_a , ε_f and ε_b correspond to $A_{\text{obsd}}/[\text{complex}]$, the extinction coefficient for the free complex, and the extinction coefficient for the complex in the fully bound form, respectively. The intrinsic binding constant (K_b) values of 2.47×10^4 for **1** and 3.04×10^4 for **2** were obtained following the above equation. This suggests that the ligands of *o*-NPIP and *p*-CPIP exhibit a similar intercalative binding effect even with different space configurations and positions for the substituents of NO₂ and Cl on the phenyl ring. This suggests that the ligand of *o*-NPIP exhibits a stronger intercalative binding effect than *p*-CPIP. The interactions of complexes (**1** and **2**) with DNA have shown that the complexes are electron-acceptors and the DNA molecule is the electron-donor. NO₂ is a powerful electron-withdrawing group than the Cl group, which can accept electrons from DNA. So ligand *o*-NPIP shows strong binding ability towards CT-DNA.

Fluorescence spectroscopic methods. No luminescence is observed for **1** and **2** at room temperature in aqueous solution, in any organic solvent examined, or in the presence of CT-DNA. To further clarify the interaction of the complexes with DNA, the competitive binding experiment was carried out by adding EB, which is well known to be a typical indicator of the intercalation probe. In the presence of CT-DNA, EB can intercalate the planar phenanthridinium ring between adjacent base pairs of the double helix and emit strong fluorescence.³⁶ It was reported that this enhanced fluorescence could be quenched by adding another kind of molecules,³⁷ so the changes in the spectra of the EB–DNA system are often used for the interaction study between DNA and metal complexes. The emission spectra of EB–DNA in the

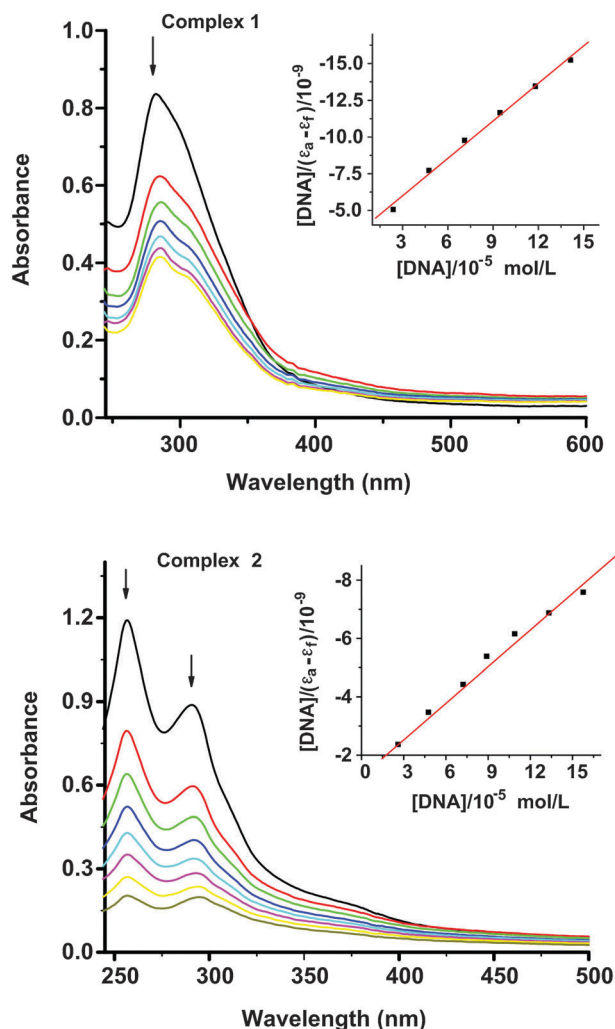


Fig. 2 Absorption spectra of **1** and **2** (47.6 μM) in the absence and presence of increasing amounts of CT-DNA at room temperature in Tris-HCl/NaCl buffer (pH = 7.2). Inset: plot of $[\text{DNA}]/(\epsilon_a - \epsilon_f)$ vs. $[\text{DNA}]$ for absorption titration of CT-DNA with complexes.

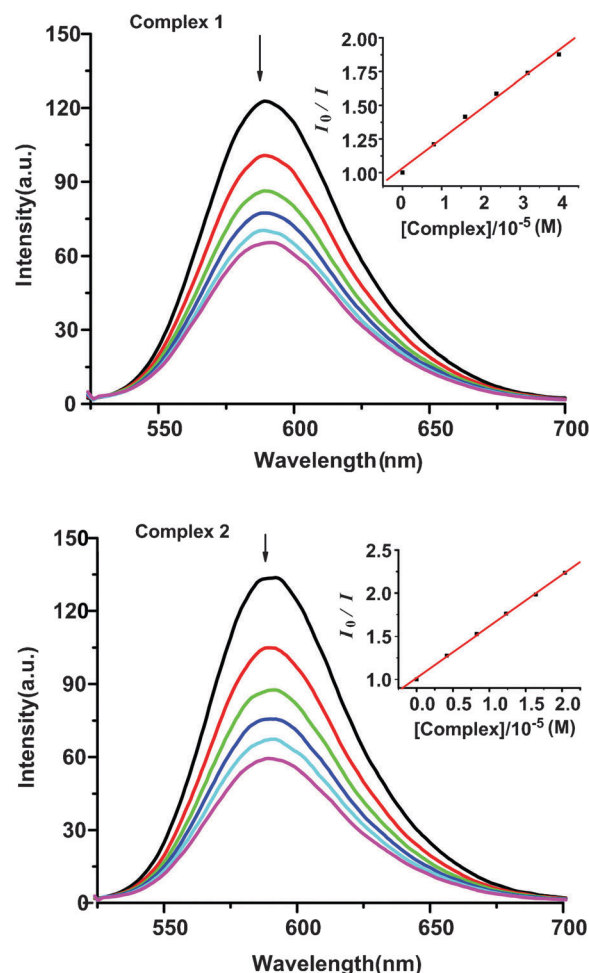


Fig. 3 Fluorescence quenching curves of EB bound to CT-DNA by **1** and **2** ($[\text{complex}] = 0\text{--}30.2 \mu\text{M}$, $\lambda_{\text{ex}} = 510 \text{ nm}$). The arrow shows the intensity changes on increasing the complex concentration. Inset: plot of I_0/I vs. $[\text{complex}]$.

absence and presence of **1** and **2** are given in Fig. 3. The addition of **1** and **2** to EB-DNA ($[\text{EB}] = 50 \mu\text{M}$ and $[\text{CT-DNA}] = 100 \mu\text{M}$) causes obvious reduction in the emission intensities, which indicates that **1** and **2** can competitively bind to CT-DNA with EB. The extent of reduction of the emission intensity gives a measure of the binding propensity of the complex to DNA according to the classical Stern-Volmer eqn (2):³⁸

$$I_0/I = 1 + K_{\text{sv}}[Q] \quad (2)$$

In this expression, I_0 and I are the fluorescence intensities in the absence and presence of the quencher, respectively. K_{sv} is a linear Stern-Volmer quenching constant. $[Q]$ is the concentration of the quencher. The quenching plot illustrates that the quenching of EB-DNA by **1** and **2** is in agreement with the linear Stern-Volmer equation, which also indicates that **1** and **2** effectively bind to CT-DNA as can be seen from eqn (3):

$$K_{\text{EB}}[\text{EB}] = K_{\text{app}}[\text{complex}] \quad (3)$$

In this expression, $[\text{complex}]$ is the value of a 50% reduction of the fluorescence intensity of EB and $K_{\text{EB}} = 1.0 \times 10^7 \text{ M}$, $[\text{EB}] = 50 \mu\text{M}$. The apparent binding constants (K_{app}) at room temperature are calculated to be $4.97 \times 10^5 \text{ M}^{-1}$ for **1** and $1.45 \times 10^6 \text{ M}^{-1}$ for **2**, less than the binding constant of the classical intercalators and metallointercalators (10^7 M^{-1}).³⁹ The results show that both **1** and **2** have moderate intercalative ability to CT-DNA. The results show that DNA EB-competitive binding of **2** is stronger than that of **1**, which is consistent with the previous absorption spectral measurement results.

DNA cleavage studies. In order to estimate the chemical nuclease activities of the copper complexes for DNA strand scission, pUC19 DNA in a medium of 50 mM Tris-HCl/NaCl buffer (pH = 7.2) in the absence and presence of **1** and **2** under the physiological conditions was chosen. The DNA cleavage study was conducted by gel electrophoresis. The cleavage activities could be assessed by the conversion of DNA from the original supercoiled form (Form I) to the nicked form (Form II, single-strand breaks, SSBs) and the linear form (Form III, double-strand breaks, DSBs). When pUC19 DNA is subject to

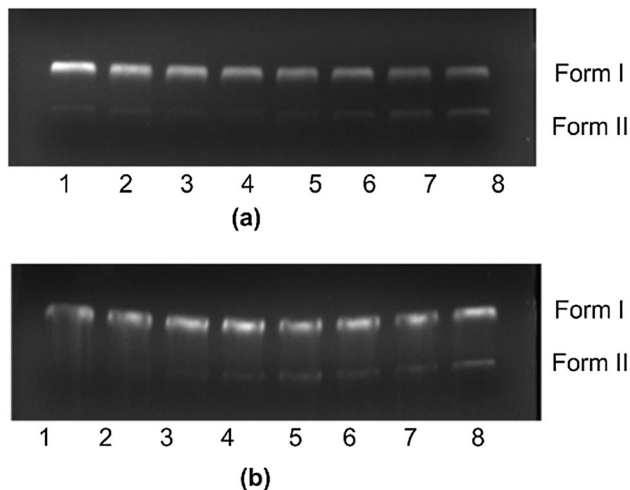


Fig. 4 (a) Gel electrophoresis diagrams showing cleavage of pUC19 DNA ($0.1 \mu\text{g } \mu\text{L}^{-1}$) by **1** in Tris-HCl/NaCl buffer (pH = 7.2) at different concentrations for 3 h at 37°C . Lane 1: DNA control; lanes 2–8: DNA + **1** (2.08, 6.25, 14.56, 20.80, 27.04, 35.36 and $42.25 \mu\text{M}$). (b) Gel electrophoresis diagrams showing cleavage of pUC19 DNA ($0.1 \mu\text{g } \mu\text{L}^{-1}$) by **2** under the same conditions as above. Lane 1: DNA control; lanes 2–8: DNA + **2** (0.42, 1.25, 2.92, 4.17, 5.42, 7.08 and $8.28 \mu\text{M}$).

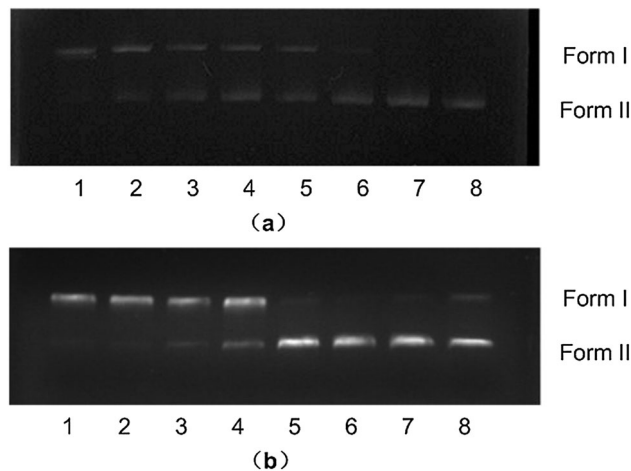


Fig. 5 (a) Gel electrophoresis diagrams showing cleavage of pUC19 DNA ($0.1 \mu\text{g } \mu\text{L}^{-1}$) by **1** in Tris-HCl/NaCl buffer (pH = 7.2) at different concentrations for 3 h at 37°C . Lane 1: DNA control; lane 2: DNA + H_2O_2 ($1 \times 10^{-5} \mu\text{M}$); lanes 3–8: DNA + H_2O_2 + **1** (2.08, 6.25, 14.56, 20.80, 27.04 and $35.36 \mu\text{M}$). (b) Gel electrophoresis diagrams showing cleavage of pUC19 DNA ($0.1 \mu\text{g } \mu\text{L}^{-1}$) by **2** under the same conditions as above. Lane 1: DNA control; lane 2: DNA + H_2O_2 ($1 \times 10^{-5} \mu\text{M}$); lanes 3–8: DNA + H_2O_2 + **2** (0.42, 1.25, 2.92, 4.17, 5.42 and $7.08 \mu\text{M}$).

electrophoresis, relatively fast migration was observed for Form I, slower migration for Form II, and Form III appeared between Form I and Form II.

Firstly, the concentration dependent DNA cleavage by complexes **1** and **2** was performed. As shown in Fig. 4, with the increase of the complexes concentration, Form I did not convert into Form II and Form III. So the results indicate that complexes **1** and **2** have not exhibited effective nuclease activity towards pUC19 DNA only by themselves. Besides a few examples of hydrolytic cleavage, most of the DNA cleavages were mediated by the copper complexes *via* an oxidative mechanism.⁴⁰ Sigman *et al.*⁴¹ have found that the 1,10-phenanthroline copper(II) complex induced DNA cleavage in the presence of oxygen or H_2O_2 . H_2O_2 acts as an activator and can generate reactive oxygen species (ROS) or reactive metal-oxo species (RMOS) upon reaction with copper, which triggers the degradation of nucleic acids.⁴² Therefore, we investigated the cleavage activity of the two copper complexes in the presence of H_2O_2 . Fig. 5 shows that the supercoiled plasmid DNA is effectively converted into Form II, which showed that both complexes **1** and **2** exhibited higher oxidative DNA cleavage activity upon treatment with H_2O_2 .

DNA cleavage mechanism. To check the effects of active oxygen species on DNA damage, we investigated the DNA cleavage in the presence of a hydroxyl radical scavenger (DMSO), singlet oxygen quenchers (NaN_3 and L-histidine), a superoxide scavenger (SOD), a chelating agent (EDTA) and a hydrogen peroxide scavenger (KI),⁴³ respectively, under the experimental conditions. No obvious inhibition is observed for **1** in the presence of SOD (lane 5) as shown in Fig. 6a, which suggests that the superoxide scavenger is not involved in the cleavage process. And for **2**, SOD and L-histidine have no effect on the cleavage reaction (lanes 5 and 8) (Fig. 6b), which indicates that the superoxide scavenger and singlet oxygen

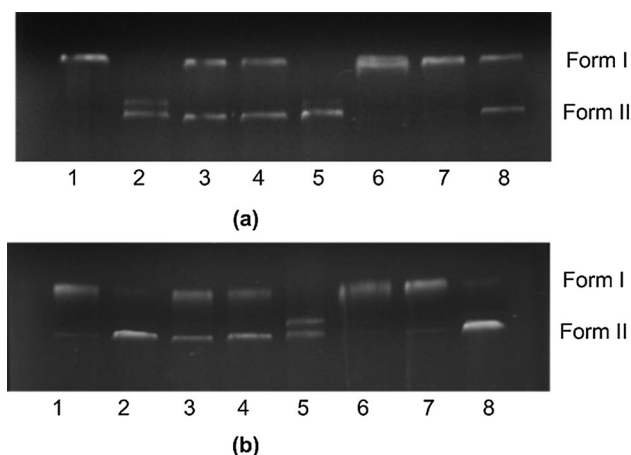


Fig. 6 (a) Agarose gel showing cleavage of pUC19 DNA ($0.1 \mu\text{g } \mu\text{L}^{-1}$) incubated by **1** ($35.36 \mu\text{M}$) in Tris-HCl/NaCl buffer (pH = 7.2) at 37°C for 3 h. Lane 1: DNA control; lane 2: DNA + H_2O_2 ($1 \times 10^{-5} \mu\text{M}$); lane 3: DNA + H_2O_2 + 20 mM DMSO; lane 4: DNA + H_2O_2 + 20 mM NaN_3 ; lane 5: DNA + H_2O_2 + 20 U mL^{-1} SOD; lane 6: DNA + H_2O_2 + 5 mM EDTA; lane 7: DNA + H_2O_2 + 20 mM KI; lane 8: DNA + H_2O_2 + 20 mM L-histidine. (b) Agarose gel showing cleavage of pUC19 DNA ($0.1 \mu\text{g } \mu\text{L}^{-1}$) incubated with **2** ($7.08 \mu\text{M}$) in Tris-HCl/NaCl buffer (pH = 7.2) at 37°C for 3 h. Lane 1: DNA control; lane 2: DNA + H_2O_2 ($1 \times 10^{-5} \mu\text{M}$); lane 3: DNA + H_2O_2 + 20 mM DMSO; lane 4: DNA + H_2O_2 + 20 mM NaN_3 ; lane 5: DNA + H_2O_2 + 20 U mL^{-1} SOD; lane 6: DNA + H_2O_2 + 5 mM EDTA; lane 7: DNA + H_2O_2 + 20 mM KI; lane 8: DNA + H_2O_2 + 20 mM L-histidine.

are not involved in the cleavage process. When EDTA (lane 6) (Fig. 6a and b) was added to the reaction mixture, the DNA cleavage mediated by both **1** and **2** was strongly inhibited, confirming that the chelating agent is the intermediate that participates in the DNA scission process. The results showed

that the EDTA, a Cu(II)-specific chelating agent that strongly binds to Cu(II) forming a stable complex, can efficiently inhibit DNA cleavage, indicating that Cu(II) complexes play a key role in the cleavage process. For the copper complexes oxidative DNA cleavage, it is proposed that Cu²⁺ is reduced to Cu¹⁺ species by a reductant, and Cu¹⁺ species form ROS subsequently by reacting with O₂ or H₂O₂.⁴⁴ In our work, H₂O₂ acts as the reductant in the absence of other reductants and a coreactant with Cu¹⁺.⁴² It is the origin for EDTA quenching the Cu-induced DNA scission. KI (lane 7) (Fig. 6a and b) significantly inhibited the DNA cleavage activity of the two complexes, which indicated the involvement of hydrogen peroxide in the cleavage process. This phenomenon could be explained by the inhibitory effect of EDTA on DNA scission.

BSA studies

Fluorescence spectroscopy of BSA. Studies on the interactions between metal complexes and proteins are of great importance for investigating the mechanism of transport and metabolism. Furthermore, the binding of metal complexes to proteins may provide information on the relationship between structures and functions of proteins.

Qualitative analysis of binding of metal compounds to BSA can be performed by examining fluorescence spectra. The emission spectra of BSA in the presence of increasing concentrations of **1** and **2** are recorded in the wavelength range 300–500 nm by exciting the protein at 290 nm. Fig. 7 shows that the fluorescence intensities of BSA obviously decrease with increasing concentrations of **1** and **2**, which indicate that **1** and **2** can effectively bind to the proteins. Commonly, fluorescence quenching can be described by the following Stern–Volmer eqn (4).³⁸

$$F_0/F = 1 + K_q\tau_0[Q] = 1 + K_{sv}[Q] \quad (4)$$

In this equation, F_0 and F represent the fluorescence intensities in the absence and presence of the quencher, respectively. K_q is the quenching rate constant of the biomolecule, K_{sv} is the dynamic quenching constant, τ_0 is the average life-time of the biomolecule without the quencher ($\tau_0 = 6.2$ ns) and $[Q]$ is the concentration of quencher. Fig. 8 displays the Stern–Volmer plots of the quenching of BSA emission fluorescence by **1** and **2** at different temperatures. Fluorescence quenching can occur by different mechanisms, which are usually classified as dynamic quenching and static quenching. The dynamic and static quenching can be distinguished by their differing dependence on temperature. In the case of dynamic quenching, higher temperature results in faster diffusion, and consequently, the quenching rate constant increases with the increasing temperature. In contrast, in the case of static quenching, increasing temperature will result in decreasing complex stability and hence in lowering of the value of the static quenching constant.⁴⁵ The corresponding Stern–Volmer quenching constant K_{sv} and the quenching rate constant K_q are given in Table 3. The results show that the corresponding Stern–Volmer quenching constant K_{sv} increases with the rising temperature, indicating that the fluorescence quenching of BSA by **1** and **2** is likely to occur by a dynamic quenching mechanism. While the obtained bimolecular

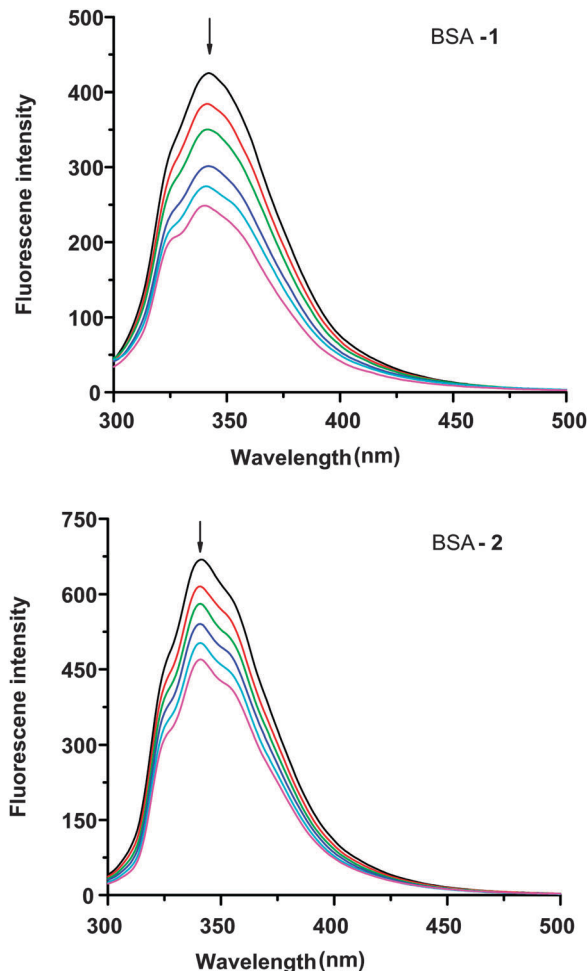


Fig. 7 Fluorescence spectra of BSA in the different concentrations of **1** and **2** at room temperature. The concentrations of BSA are: (5×10^{-7} M), complex **1** (0–3 μ M) and complex **2** (0–4 μ M), respectively.

quenching constant K_q for **1** and **2** is on the order of 10^{13} L mol⁻¹ s⁻¹, which is 1000-fold higher than the maximum value possible for diffusion controlled quenching (*i.e.* 2.0×10^{10} L mol⁻¹ s⁻¹).⁴⁶ This observation suggests that the quenching is not initiated by dynamic collision but by a static one. So we have to continue exploring the quenching mechanism by UV-vis spectra.

UV-vis spectroscopy. UV-vis absorption measurement is a simple but effective method for detecting formation of complex formation. In a dynamic quenching mechanism, with the addition of a quencher, only the excited state fluorescence molecule is affected, which results in no change in the absorption spectra of BSA. While, in a static quenching, a new compound is formed between BSA and the quencher, therefore, the absorption spectra of BSA would be considerably affected. It appears that the UV absorption peak goes up or down. The influences of the absorbance of BSA were observed by adding the same concentration of **1** and **2**. From Fig. 9, we can see that BSA absorption peaks at around 280 nm due to the presence of aromatic amino acids (Trp, Tyr, and Phe) exist.⁴⁷ For **1**, the absorption spectra of BSA did not change, indicating that **1** and BSA did not form a new compound. While the absorption spectra increased with adding **2**, indicating that

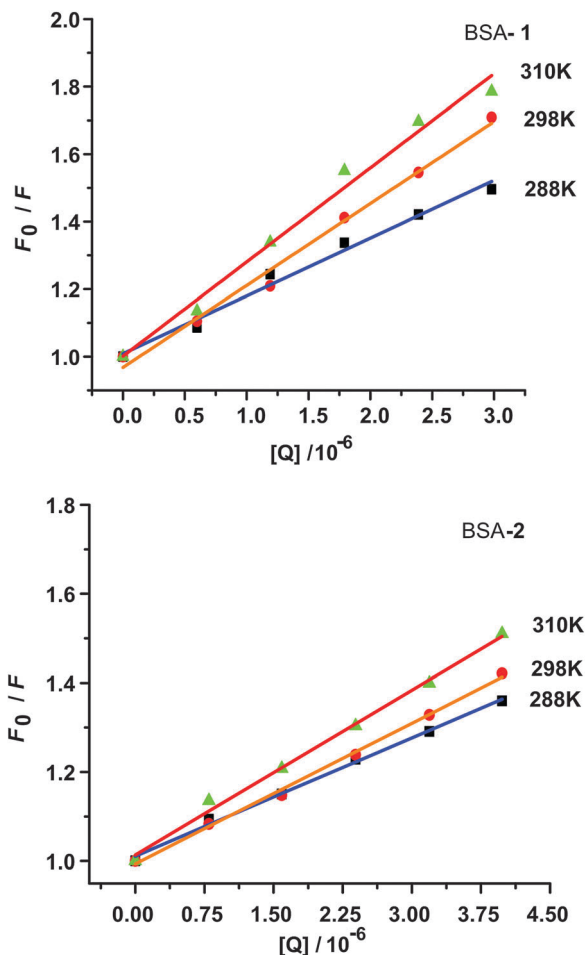


Fig. 8 The Stern–Volmer plots of the fluorescence quenching of BSA by **1** and **2** at different temperatures ($T = 288, 298$ and 310 K). Inset: plot of F_0/F vs. [complex].

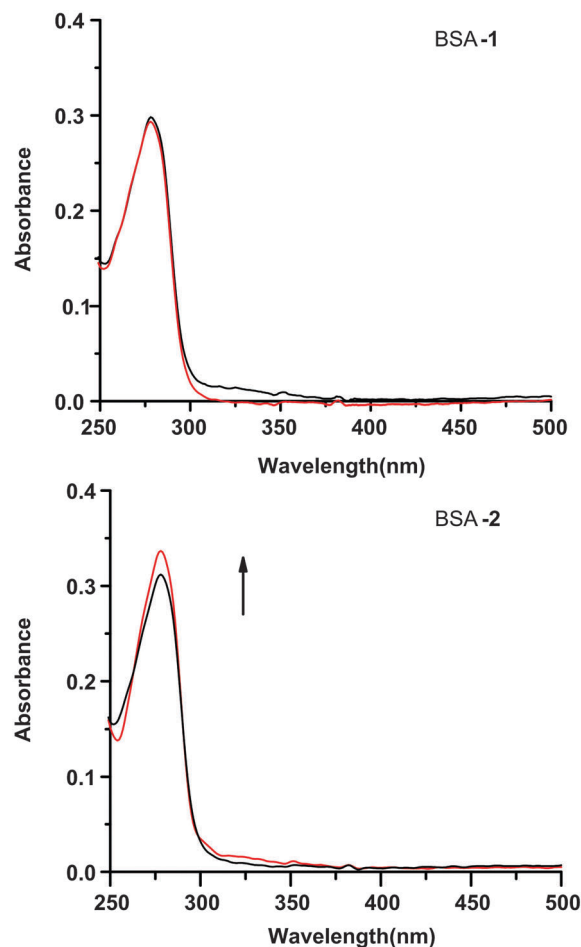


Fig. 9 UV-vis absorption spectra of BSA in the absence and presence of **1** and **2**. Black line: the absorption spectrum of BSA. Red line: the absorption spectrum of BSA in the presence of **1** or **2** at the same concentration, c (BSA) = c (**1** or **2**) = 5×10^{-7} M.

Table 3 The quenching constants (K_{sv} and K_q), binding constant (K_b), the number of binding sites (n) of the BSA-**1** and BSA-**2** systems at different temperatures

| | T (K) | $K_{sv} \times 10^5$ (1 mol^{-1}) | $K_q \times 10^{13}$ (1 mol^{-1}) | $K_b \times 10^5$ (1 mol^{-1}) | n |
|----------|---------|--|--|---|------|
| 1 | 288 | 1.70 | 2.74 | 1.69 | 1.07 |
| | 298 | 2.43 | 3.92 | 1.88 | 1.21 |
| | 310 | 2.79 | 4.50 | 2.80 | 1.12 |
| 2 | 288 | 0.87 | 1.43 | 1.09 | 0.85 |
| | 298 | 1.05 | 1.69 | 1.23 | 1.20 |
| | 310 | 1.98 | 1.98 | 1.53 | 0.83 |

the microenvironment of the three aromatic acid residues was changed and the tertiary structure of BSA was destroyed, and this can prove that **2** and BSA formed a novel complex. These results show that the quenching mechanism of **1** is mainly a dynamic quenching process, and that of **2** is a combined process, in which dynamic and static quenching mechanisms are concurrent. It suggested that the polypyridyl ligand, which was modified by the substituent group at different sites probably, can create some interesting differences in the space configurations and

the electronic structures. So it is the possible reason why the binding mode between complex **2** and BSA is different from complex **1**.

Binding constants and the number of binding sites. It is assumed that there are independent binding sites in the biomolecule. The binding constant (K_b) and the number of binding sites (n) can be determined by using the double logarithm eqn (5):⁴⁸

$$\log((F_0 - F)/F) = \log K_b + n \log[Q] \quad (5)$$

In this equation, F_0 and F are the fluorescence intensities presence and absence **1** and **2**, respectively; $[Q]$ is the total concentration of **1** and **2**, K_b is the binding constant for the complex–protein interaction and n is the number of binding sites per albumin molecule. As seen from Fig. S2 (ESI[†]), the binding constant increases with the rising temperature, indicating that the capacity of **1** and **2** to bind to BSA is enhanced with the increasing temperature. The values of n at the experimental temperature are approximately equal to one, which indicates that there is just one independent binding site in BSA for **1** and **2** (Table 3).

Synchronous fluorescence spectroscopy studies. It is reported that synchronous fluorescence spectroscopy is frequently used to characterize the interaction between the fluorescence probe and proteins,⁴⁹ because this technique can provide information about the molecular environment in the vicinity of the fluorophore molecules.⁵⁰ The synchronous fluorescence spectroscopy involves the simultaneous scanning of excitation and emission spectra on a fluorimeter, while maintaining a fixed wavelength difference ($\Delta\lambda$) between them. When $\Delta\lambda$ is stabilized at 15 nm, the synchronous fluorescence gives the characteristic information of tyrosine residues, whereas $\Delta\lambda$ of 60 nm indicates that of tryptophan residues.⁵¹ The maximum emission wavelengths of tryptophan and tyrosine residues are related to the polarity of their surroundings. When the wavelengths change, it can be inferred that the protein conformation is changed. From Fig. S4 (ESI[†]), it can be seen that upon addition of **1** and **2**, the maximum emission wavelength shows no shift when $\Delta\lambda$ was equal to 15 nm. However, as seen from Fig. S5 (ESI[†]), the maximum emission wavelength represents obviously red shift when $\Delta\lambda$ was equal to 60 nm. The red shift indicates that the conformation of BSA was changed while the polarity around the tryptophan residues increased, whereas the hydrophobicity decreased.⁵²

Conclusion

In this work, we have synthesized and characterized two Cu(II) polypyridyl complexes to study the selectivity and efficiency of DNA recognized and cleaved by binuclear Cu(II) complexes. The interaction of complexes with calf thymus DNA (CT-DNA) was investigated by UV-visible and fluorescence emission spectrometry, as well as agarose gel electrophoresis. Results suggest moderate intercalative binding mode between the complexes and DNA. Both **1** and **2** exhibited effective oxygen DNA cleavage activity in the absence of external agents such as H₂O₂. DNA cleavage mechanism studies show that both **1** and **2** might be capable of promoting DNA cleavage through oxidative DNA damage pathways. According to the results obtained from fluorescence spectrometry of BSA, we conclude that the fluorescence quenching of BSA by **1** is a dynamic quenching process because K_{sv} increases with increasing temperature. UV absorption spectra show that **2** involves a combined process, in which dynamic and static quenching mechanisms are concurrent. The details of the binding mode, specific binding sites and energy transfer upon BSA binding with complexes are not very clear at present and further studies are currently in progress.

Acknowledgements

The work was supported by the NSFC (China) (No. 21371135) and the Key Program of Tianjin Municipal Natural Science Foundation (China) (No. 13JCZDJC28200).

References

- 1 K. E. Erkkila, D. T. Odom and J. K. Barton, *Chem. Rev.*, 1999, **99**, 2777–2795.

- 2 X. J. Li, K. Zheng, L. D. Wang, Y. T. Li, Z. Y. Wu and C. W. Yan, *J. Inorg. Biochem.*, 2013, **128**, 97–107.
- 3 R. K. Ameta, M. Singh and R. K. Kate, *New J. Chem.*, 2013, **37**, 1501–1508.
- 4 A. Tarushi, J. Kljun, I. Turel, A. A. Pantazaki, G. Psomas and D. P. Kessisoqlou, *New J. Chem.*, 2013, **37**, 342–355.
- 5 G. Pratviel, J. Bernadou and B. Meunier, *Adv. Inorg. Chem.*, 1998, **45**, 251–312.
- 6 H. T. Chifotides and K. R. Dunbar, *Acc. Chem. Res.*, 2005, **38**, 146–156.
- 7 V. G. Vaidyanathan and B. U. Nair, *Dalton Trans.*, 2005, 2842–2848.
- 8 L. F. Tan, F. Wang, H. Chao, Y. F. Zhou and C. Weng, *J. Inorg. Biochem.*, 2007, **101**, 700–708.
- 9 L. N. Ji, X. H. Zou and J. G. Liu, *Coord. Chem. Rev.*, 2001, **216–217**, 513–536.
- 10 A. Nori and J. Kopecek, *Adv. Drug Delivery Rev.*, 2005, **57**, 609–636.
- 11 R. M. Burger, *Chem. Rev.*, 1998, **98**, 1153–1169.
- 12 M. Morshedi and H. Hadadzadeh, *J. Fluoresc.*, 2013, **23**, 259–264.
- 13 T. W. Hambley, *Dalton Trans.*, 2007, 4929–4937.
- 14 C. H. Ng, W. S. Wang, K. V. Chong, Y. F. Win, K. E. Neo, H. B. Lee, S. L. San, R. Abd Rrhmand and W. K. Leonge, *Dalton Trans.*, 2013, **42**, 10233–10243.
- 15 Y. Lu, *Chem.–Eur. J.*, 2002, **8**, 4588–4596.
- 16 J. K. Barton, A. T. Danishefsky and J. M. Goldberg, *J. Am. Chem. Soc.*, 1984, **106**, 2172–2176.
- 17 B. M. Goldstein, J. K. Barton and H. M. Berman, *Inorg. Chem.*, 1986, **25**, 842–847.
- 18 Y. J. Liu, C. H. Zeng, H. L. Huang, L. X. He and F. H. Wu, *Eur. J. Med. Chem.*, 2010, **45**, 564–571.
- 19 Q. L. Zhang, J. G. Liu, H. Xu, H. Li, J. Z. Liu, H. Zhou, L. H. Qu and L. N. Ji, *Polyhedron*, 2001, **20**, 3049–3055.
- 20 S. Shi, J. Liu, J. Li, K. C. Zheng, C. P. Tan, L. M. Chen and L. N. Ji, *Dalton Trans.*, 2005, 2038–2046.
- 21 Y. X. Ma, L. Cao, T. Kawabata, T. Yoshino, B. B. Yang and S. Okada, *Free Radical Biol. Med.*, 1998, **25**, 568–575.
- 22 S. Y. Tsang, S. C. Tam, I. Bremner and M. J. Burkitt, *Biochem. J.*, 1996, **317**, 13–16.
- 23 B. X. Huang and H. Y. Kim, *J. Am. Soc. Mass Spectrom.*, 2004, **15**, 1237–1247.
- 24 N. Shahabadi, M. Maghsudi, Z. Kiaani and M. Pourfoulad, *Food Chem.*, 2001, **124**, 1063–1068.
- 25 Y. N. Hu, X. S. Shen, X. Y. Fang and S. S. Qu, *J. Mol. Struct.*, 2005, **738**, 143–147.
- 26 R. A. Alderden, M. D. Hall and T. W. Hambley, *J. Chem. Educ.*, 2006, **83**, 728.
- 27 C. Marzano, A. Trevisan, L. Giovagnini and D. Fregona, *Toxicol. In Vitro*, 2002, **16**, 413–419.
- 28 A. I. Matesanz, C. Hernández, A. Rodríguez and P. Souza, *Dalton Trans.*, 2011, **40**, 5738–5745.
- 29 C. L. Liu, M. Wang, T. L. Zhang and H. Z. Zhe, *Coord. Chem. Rev.*, 2004, **248**, 147–168.
- 30 H. Xu, K. C. Zheng, Y. Chen, Y. Z. Li, L. J. Lin, H. Li, P. X. Zhang and L. N. Ji, *Dalton Trans.*, 2003, 2260–2268.

- 31 G. M. Sheldrick, *SHELXS-97, Program for the Solution of Crystal Structure*, University of Göttingen, Germany, 1997.
- 32 J. A. Simpson, K. H. Cheeseman, S. E. Smith and R. T. Dean, *Biochem. J.*, 1988, **254**, 519–523.
- 33 A. W. Addison, T. Nageswara Rao, J. Reedijk, J. van Rijn and G. C. Verschoor, *J. Chem. Soc., Dalton. Trans.*, 1984, 1349–1356.
- 34 S. A. Tysoe, R. J. Morgan, A. D. Baker and T. C. Streckas, *J. Phys. Chem.*, 1993, **97**, 1707–1711.
- 35 A. M. Pyle, J. P. Rehmann, R. Meshoyrer, C. V. Kumar, N. J. Turro and J. K. Barton, *J. Am. Chem. Soc.*, 1989, **111**, 3051–3058.
- 36 F. J. Meyer-Almes and D. Porschke, *Biochemistry*, 1993, **32**, 4246–4253.
- 37 A. Wolf, G. H. Shimer Jr and T. Meehan, *Biochemistry*, 1987, **26**, 6392–6396.
- 38 J. R. Lakowicz and G. Weber, *Biochemistry*, 1973, **12**, 4161–4170.
- 39 M. Cory, D. D. McKee, J. Kagan, D. W. Henry and J. A. Miller, *J. Am. Chem. Soc.*, 1985, **107**, 2528–2536.
- 40 C. L. Liu, M. Wang, T. L. Zhang and H. Z. Zhe, *Coord. Chem. Rev.*, 2004, **248**, 147–168.
- 41 M. Kuwabara, C. Yoon, T. Goynes, T. Thederahn and D. S. Sigman, *Biochemistry*, 1986, **25**, 7401–7408.
- 42 Q. Jiang, N. Xiao, P. F. Shi, Y. G. Zhu and Z. J. Guo, *Coord. Chem. Rev.*, 2007, **251**, 1951–1972.
- 43 M. E. Reichmann, S. A. Rice, C. A. Thomas and P. Doty, *J. Am. Chem. Soc.*, 1954, **76**, 3047–3053.
- 44 S. Borah, M. S. Melvin, N. Lindquist and R. A. Manderville, *J. Am. Chem. Soc.*, 1998, **120**, 4557–4562.
- 45 M. R. Eftink and C. A. Ghiron, *J. Phys. Chem.*, 1976, **80**, 486–493.
- 46 P. B. Kandagal, S. Ashoka, J. Seetharamappa, V. Vani and S. M. T. Shaikh, *J. Photochem. Photobiol., A*, 2006, **179**, 161–166.
- 47 F. Wang, W. Huang and Z. X. Dai, *J. Mol. Struct.*, 2008, **875**, 509–514.
- 48 N. Wang, L. Ye, F. F. Yan and R. Xu, *Int. J. Pharm.*, 2008, **351**, 55–60.
- 49 G. Z. Chen, X. Z. Huang, J. G. Xu, Z. Z. Zheng and Z. B. Wang, *The Methods of Fluorescence Analysis*, Beijing Science Press, 1990, pp. 2–112.
- 50 J. Jayabharathi, V. Thanikachalam and M. V. Perumal, *Spectrochim. Acta, Part A*, 2011, **79**, 502–507.
- 51 C. W. Fuller and J. N. Miller, *Proc. Anal. Div. Chem. Soc.*, 1979, **16**, 199–208.
- 52 G. C. Zhang, Y. Q. Wang, H. M. Zhang, S. H. Tang and W. H. Tao, *Pestic. Biochem. Physiol.*, 2007, **87**, 23–29.